Fundamentals and advances in thermal transport in thermoelectric materials

Keivan Esfarjani* and Junichiro Shiomi

This article attempts to summarize our understanding of heat flow in different solid materials and its relationship to atomistic structure of materials. This knowledge can be used to understand and design materials for electricity generation or cooling through the thermoelectric effect. We start with the fundamentals of heat transport in solids: mechanisms of phonon scattering in crystals, the role of interfaces and coherence, and the relationship between chemical bonding and heat transport will be elucidated. Theories used to model thermal conductivity of solids will be exposed next. They include the Green–Kubo formulation, Boltzmann transport equation and its recent quantum extensions, and Allen–Feldman theory of heat diffusion in noncrystalline solids and its recent extensions. In terms of phenomenology, we will distinguish between the kinetic regime based on independent single carriers and the collective or hydrodynamic one which occurs when normal or momentum-conserving processes dominate. Next, we will focus on advanced measurement and characterization techniques, and the knowledge extracted from them. Nanoscale thermal conductivity methods, such as the pump-probe thermoreflectance methods (TDTR/FDTR), have become fairly common allowing researchers to measure thermal conductivity of thin-film thermoelectrics. We will review recent advances of the method: the Gibbs excess approach, which measures thermal resistance across a grain boundary of polycrystals through mapping TDTR/FDTR measurements, and the transient Raman method, where pump-probe Raman spectroscopy realizes in-plane thermal conductivity measurements of two-dimensional materials even on a substrate. We will also review the progress in mode-resolved phonon property measurements, such as inelastic x-ray scattering for thin-film samples, which allows direct observation of the modulation of phonon band and lifetime by nanostructures, and thermal diffuse scattering for quick characterization of phonon dispersion relations. Finally, because the main focus of this issue is thermoelectrics, we will review different classes of materials and strategies to lower their thermal conductivities.

Introduction

In thermoelectric materials, the ability to carry an electric current under an applied temperature gradient is a measure of the efficiency of a material to convert heat or rather temperature difference, to electrical energy. The efficiency is high if the Seebeck coefficient, defined as the ratio of voltage difference to temperature difference across the sample under open-circuit condition, is large and if the electrical conductivity is large at the same time. If, however, the thermal conductivity is not small, one cannot sustain a large temperature gradient across the sample, and this limits the created voltage. High thermoelectric efficiency therefore also requires a small thermal conductivity.

The basic understanding of heat transport in solid materials is based on the Fourier Law, relating the heat flux to the applied temperature gradient through a coefficient which is called the thermal conductivity: $J_Q = -\kappa \nabla T$.

In this equation, the temperature gradient is assumed to be small so that the relationship is linear and the thermal conductivity in a homogeneous sample can only be a function of the local temperature. In anisotropic materials, the latter is in general a second rank tensor. It was first predicted by Casimir in 1938,[1] and then by Callaway in 1959,[2] that κ can be size dependent, highlighting the importance of boundary scattering of phonons at small scales and temperatures. This was later confirmed experimentally in silicon thin films by Asheghi et al. in 1997.[3,4] The explanation of this phenomenon has been traced back to the ratio of the mean free path (MFP) of the heat carriers as compared with the sample size. The diffusive regime is the regime in which all carrier MFPs are smaller than the sample size, so that carriers undergo many resistive scatterings before reaching the other end of the sample. The opposite limit is the ballistic regime where most heat carriers

Keivan Esfarjani, Department of Materials Science and Engineering and Department of Physics, University of Virginia, Charlottesville, USA; k1@virginia.edu
Junichiro Shiomi, Department of Mechanical Engineering, The University of Tokyo, Tokyo, Japan; shiomi@photon.t.u-tokyo.ac.jp
*Corresponding author
doi:10.1557/s43577-025-00951-6

© The Author(s) 2025

do not undergo resistive scattering, either because their MFP is too long or their longitudinal momentum is not destroyed after a scattering process. This limit is similar to the radiation regime,[1] except that the carriers are phonons instead of photons. Because the contribution of a full MFP in the diffusive limit is replaced by the sample length, which is a fraction of the MFP, in the ballistic or boundary scattering-limited regime, the transferred heat is less in the latter case, and the thermal conductivity becomes an increasing function of sample length.

More generally, to highlight the influence of boundary scattering and size effects, three different transport regimes of heat transport are distinguished: Diffusive, hydrodynamic, and ballistic. While in the former, the thermal conductivity does not depend on the sample size, in the latter two, it varies with the dimensions of the sample, when it becomes on the order of phonon mean free paths. But before getting into the details of these regimes, let us first consider the nature of heat carriers, their kinetics, and dynamics. This is based on the language of quasiparticles, which are single-particle excitations of the quantum system. In the case of vibrational modes of perfect crystals, we refer to phonons. While discussing the solution to the Boltzmann transport equation or BTE, it is assumed that the quasiparticle lifetimes τ are longer than their inverse frequency (i.e., $\omega\tau \gg 1$). The lifetime is defined as the average time before the phonon changes to another state because of a "collision" or "scattering" event. Alternatively, but equivalently, one can say that the wavelength associated with the quasiparticle must be much smaller than its mean free path. Therefore the BTE language where phonons are treated as quasiparticles is not appropriate for strongly damped oscillations, and in this case one needs to start from first principles (i.e., the Green–Kubo definition of the thermal conductivity valid in all cases or the Wigner formulation valid for both particles and waves present in disordered systems). In disordered systems, the taxonomy will change from phonons to propagons and additional excitations called diffusons and locons.[5]

Heat carriers and their kinetics and dynamics

A simple understanding of the thermal conductivity can be achieved by considering the simple formula from kinetic theory: $\kappa = Cvl/3$, where C is the heat capacity per unit volume, v is the carrier velocity, and l its MFP, which is defined as the average distance traveled by the carrier between two successive collisions. This simple formula shows fast carriers with long MFPs can carry a lot of heat per unit time, unit area, and per unit of temperature gradient.

In metals, most of the heat is carried by electrons as compared to phonons or vibrational modes. While the heat capacity of the former is linear in temperature T that of phonons with a linear dispersion is cubic in T at low T and thus negligible. But at high temperatures, due to Dulong and Petit's Law, the heat capacity per atom is less or on the order of 3 k_B, while the electronic contribution is on the order of $k_B \times (k_B T\,\mathrm{DOS}(E_F))$ per atom. In a good metal such as copper, the density of states at the Fermi level $\mathrm{DOS}(E_F) \simeq 0.5\,\mathrm{eV/atom}$, so that at room temperature $k_B T\,\mathrm{DOS}(E_F) \simeq 0.01/\mathrm{atom}$. Even though the heat capacity of an electron becomes 100 times smaller than that of a phonon at high T, the much larger group velocity of electrons ($\simeq 1000\,\mathrm{km/s}$) dominates that of phonons ($< 10\,\mathrm{km/s}$) leading to a dominant contribution of electrons to the thermal conductivity in a metal. Traditionally, one has looked for good thermoelectrics among nonmetals in the hope that the thermal conductivity can be made as small as possible.

Looking at the kinetic formula, we see that materials with phonons of short MFPs and low speeds (soft material with small elastic moduli) are favorable for low thermal conductivity. To lower thermal conductivity, one is required to create as many collisions as possible to lower MFP. There are three sources of collisions: sample boundaries, point or extended defects, and other carriers. The latter collision process is called intrinsic, whereas the two former are called extrinsic. In an insulator carriers are dominantly phonons, although one could conceive of other types of carriers such as magnons, which can collide with phonons and lead to lower phonon intrinsic MFPs, while they are also able to carry heat by themselves!

Normal versus resistive processes

Scattering processes are separated to resistive and normal. Normal processes are those that conserve momentum. As such, specular scattering against a wall, which is parallel to ∇T leads to longitudinal momentum conservation and is a nonresistive process. The terminology "normal" is reserved for only multiphonon processes that preserve total momentum. The rest of scatterings, which break longitudinal momentum conservation are called "resistive."

While nonmomentum-conserving processes, as their name indicates, cause thermal resistance, normal processes and specular reflections off a wall do not strictly lead to lower thermal conductivity. They contribute, however, to a faster randomization or equilibration of the momentum distribution but do not lead to a longitudinal momentum loss. Energy relaxation happens in multiphonon (dominantly three phonon) scatterings. Only these inelastic scatterings allow both energy (and momentum) of carriers to reach their steady-state distribution.

Different modes of phonon scattering

As previously mentioned, there are basically three types of phonon scatterings:

- *Phonon-sample boundary scattering:* these are usually elastic and thus energy conserving. Diffuse scatterings in the case of a rough surface (or interface) is nonmomentum conserving and lead to fast momentum relaxation and thermal resistance. To these scatterings one associates a rate for each phonon mode. The first nontrivial models for boundary scattering rate were developed since the 1950s by Sondheimer[6] and later adopted by several authors.[7–10] These scattering rates are constant at low frequencies and thus become dominant at very low temperatures.

- *Phonon-defect scattering:* these are also generally assumed to be energy conserving but momentum relaxing and resistive. Point defects scattering rates at very low frequencies are of Rayleigh type with a scattering rate in ω^4. This model was later improved by Tamura[11] using perturbation theory, which yielded the form $\omega^2 \mathrm{DOS}(\omega)$. More recent improvements went beyond perturbation theory, using the T-matrix approximation.[12–16] They assume scattering strength can be large, but the defect concentration is still dilute so that interference effects due to scatterings off of two or more defects are still neglected. Other types of defects are line defects such as dislocation cores or 2D manifolds such as grain and domain boundaries leading to lower powers of frequency as ω^{4-d} where $d = 1$ for lines and $d = 2$ for surfaces. In the case of dislocations, it was shown that there can also be exchange of energy with the vibrations of the dislocation core,[17] so the treatment is more complicated.[18,19] At intermediate temperatures, but typically lower than the Debye temperature, defect scatterings can become important and bring the thermal conductivity down. For strong scatterers and in the dilute limit, one needs to use the T-matrix approximation to obtain more accurate density of states and relaxation times.[20] In the case of nondilute substitutional point defects, one is in the limit of a solid solution and refers to *phonon-alloy scattering:* in solid solutions where there is crystalline order but sites are randomly occupied, the perturbation approach does not generally work. Garg et al. have proposed to use the virtual crystal as a reference and use Tamura's formula to treat alloy scattering in SiGe alloys.[21,22] In the nondilute case, the use of the coherent potential approximation or CPA[23] is preferable.
- *Phonon-other carriers scattering:* Phonons can also scatter off of other excitations of a crystal, such as electrons, polarons, polaritons, magnons, and excitons. Treating these scatterings is challenging and material dependent. But progress is being made in treating these processes when needed. The dominant process that has received the most attention is of course phonon–electron scattering.[24–26] Although this is dominant in metals, there is also a nonnegligible contribution in doped and small bandgap semiconductors where there is still a nonnegligible concentration of electrons. A notable example is $FeSb_2$, which has shown a colossal Seebeck coefficient attributed to the phonon drag effect.[27–30] Phonon drag is a nonequilibrium phenomenon that is most visible in materials with long-phonon MFPs. Under a temperature gradient, this large phonon current can, under the influence of a strong electron–phonon coupling, drag electrons and therefore create an extra voltage in addition to the regular band contribution to the Seebeck coefficient.[31–34] The main source of intrinsic phonon scattering is, however, *anharmonic phonon–phonon interactions*: At moderate temperatures, on the order of Debye or higher, the dominant anharmonic interaction is from three-phonon processes that are inelastic and thus contribute to both energy and momentum thermalization of phonons. At yet higher temperatures, phonon concentration becomes larger, and four-phonon collisions can also contribute. This process also becomes dominant if three-phonon processes are scarce. Reasons for this could be specific selection rules imposed by symmetry, such as in graphene or large acoustic–optical gap in the dispersion which prevents energy conservation in optical → acoustic + acoustic processes, but where conversion of an optical phonon to three acoustic phonons is allowed, such as in boron arsenide.[35,36] The likelihood of occurrence of these processes can be investigated by looking at the scattering phase space for mode $\omega_{k\lambda}$, which requires the knowledge of the phonon dispersion only:

$$P_3^{\pm}(\omega_{k\lambda}) = \int \frac{dk_1 dk_2 \delta(\omega - \omega_{k_1} \pm \omega_{k_2})}{\Delta(k + k_1 + k_2 + G)}, \quad (1)$$

$$P_4^{\pm,\pm}(\omega_{k\lambda}) = \int \frac{dk_1 dk_2 dk_3 \delta(\omega - \omega_{k_1} \pm \omega_{k_2} \pm \omega_{k_3})}{\Delta(k + k_1 + k_2 + k_3 + G).} \quad (2)$$

Here, P_3 and P_4 indicate the number of possible channels involving the phonon mode $\omega_{k\lambda}$ in a three-phonon and four-phonon scattering processes, respectively. The corresponding rates are essentially proportional to these phase space volumes. Anharmonic processes can either be momentum conserving or "normal" ($G = 0$) or require an additional reciprocal lattice vector to satisfy momentum conservation or "umklapp" ($G \neq 0$). For four-phonon processes, the calculation of P_4 can be an intensive computational task and Monte Carlo importance sampling as implemented in the code FOUR-PHONON[37] is advantageous. The three-phonon (normal and Umklapp), four-phonon (normal) processes as well as impurity and boundary scattering, and electron–phonon process are illustrated in **Figure** 1.

Phonon coherence in superlattices

Superlattices have been suggested by Mahan[38,39] as a strategy to make low-thermal-conductivity materials. One obvious reason is the existence of interfaces causing multiple phonon scattering. The assumption of phonon scattering at interfaces assumes incoherence across the interface, meaning the phonon identity changes when it crosses the interface (see illustration in **Figure** 2). In this case, as interface density gets larger, thermal conductivity should go down. On the other hand, one can view a clean superlattice with a short period as one bulk material with its own phonon dispersion that does not change across the interfaces. This dispersion is caused by multiple phonon reflections at interfaces and constructive interferences. In this limit of very dense interfaces or small superlattice period, thermal conductivity should go back up as interface scattering does not exist and phonons are "coherent" in the sense that they keep their identity as they cross interfaces. Thermal conductivity is then only limited by anharmonic scatterings. Consequently, one can observe

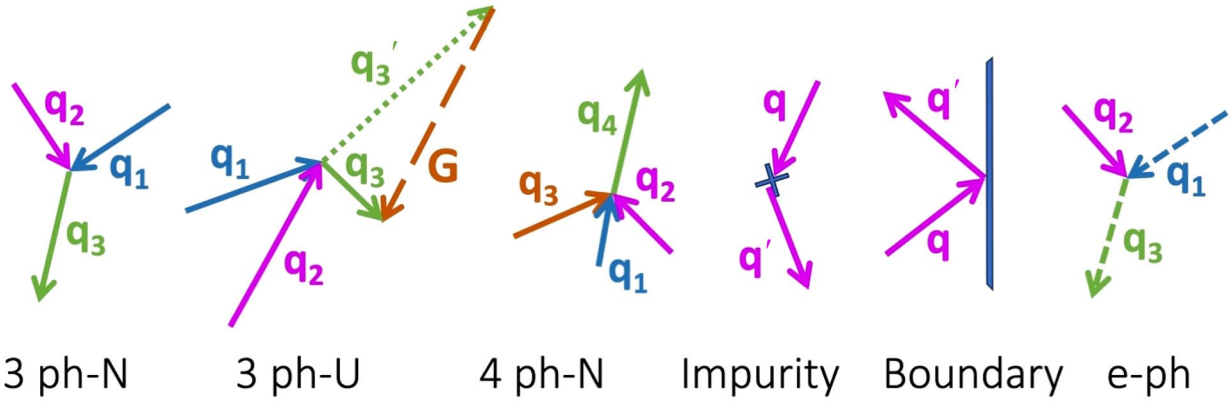

Figure 1. Different phonon scattering processes.

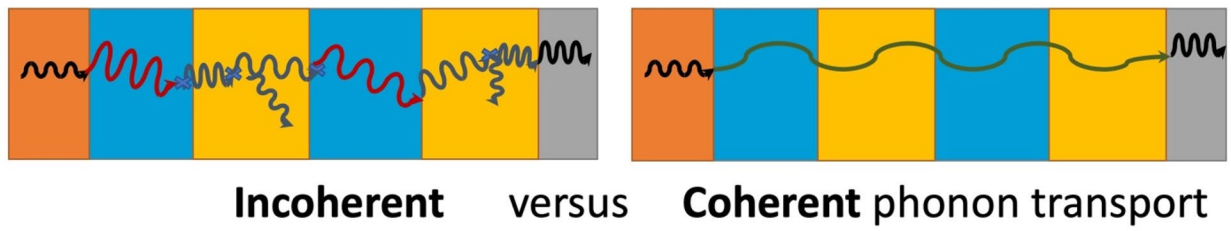

Figure 2. In the incoherent case, the identity of phonons changes across the layers.

a minimum in the thermal conductivity of a superlattice as a function of its period thickness. The necessary condition for phonon coherence is to have a clean specular interface and that the superlattice phonon MFP should be a multiple of its period, perhaps at least five periods so that multiple reflections and interferences can lead to a superlattice phonon mode. As the temperature is increased and anharmonicity lowers the MFP, coherence can be destroyed and thermal conductivity will go down. Several experiments have observed such minimum in thermal conductivity.[40–44] Evidence for the coherence was shown by Luckyanova et al.[45] who showed that, for a fixed period thickness in a GaAs–AlAs superlattice, the thermal conductivity increases almost linearly with the sample length when the latter was varied from one to nine periods. It also showed the increase in thermal conductivity with temperature, both providing evidence of coherence due to dominance of boundary (not interface) scattering in the samples.

Analysis of chemical bonds to understanding anharmonicity

Interaction potentials are a result of the effective interaction between ions mediated by the electrons. In other words, the strength of bonds has an electronic origin. There is a correlation between the dip in the potential energy and its second derivative at the minimum, which is the force constant measuring the stiffness of a bond. The deeper the energy, the larger the second derivative. On the other hand, there is a correlation[46] between bond stiffness and the so-called crystal overlap Hamiltonian population (COHP)[47] between atomic orbital α of atom j and orbital β of atom l, at eigenstate λ defined by $\mathrm{COHP}(j\alpha, l\beta; E_\lambda) = \rho_{j\alpha,l\beta}(E_\lambda)H_{j\alpha,l\beta}$, where $\rho_{j\alpha,l\beta}(E_\lambda)$ is the contribution of the eigenstate of eigenvalue (E_λ) to the density matrix, and $H_{j\alpha,l\beta}$ is the Hamiltonian matrix element between orbitals $j\alpha$ and $l\beta$. The Electronic Hamiltonian of bound electrons being negative, a negative COHP means bonding states and a positive COHP means antibonding states at the energy of interest. Strength of a bond $j-l$ can be considered to be "correlated" to $S_{jl} = \sum_{\alpha\beta,E_\lambda<E_F}\mathrm{COHP}(j\alpha, l\beta; E_\lambda)$, although this term does not include the full ion-ion repulsive part of the potential. The integral of the positive part of this quantity (i.e., the antibonding contribution) can therefore characterize the softness of the bond. The justification for this statement has been provided in a paper by Liao's group[48] where they showed that removing the effect of antibonding electrons led to stronger force constants between atom pairs and to weaker anharmonicity as evidenced by lower Grüneisen parameters and scattering rates. Now for soft bonds, because the local potential energy curvature is small, atomic displacements will be large and anharmonic portions of the potential energy landscape will be more often explored by the vibrating atom, especially at higher temperatures. In our recent work[49] where we

observed that the thermal conductivity of LaP is surprisingly lower than that of LaBi, despite its lighter mass, we explored the antibonding concept to explain the larger anharmonicity in LaP. Finally, it was traced back to the metavalent nature[50] and softness of the bonds in this compound.

Recent theoretical advances

Beyond the numerical implementations of the solution of BTE, it is important to understand the assumptions and their domain of validity. Although the standard methodologies as implemented in ALAMODE,[51,52] SHENG-BTE,[53] PHONO3PY,[54,55] and similar software is widely used by many authors, in many materials, these assumptions may be violated, leading to erroneous estimations of the MFPs less than a bond length, and thus of the thermal conductivity.

Proof of gauge invariance

In 2015, Baroni and his group showed that despite multiple choices for the definition of the heat current, the Green–Kubo formula is gauge invariant and leads to the same thermal conductivity.[56] Therefore, he designed a way to compute the heat current and thermal conductivity directly from DFT simulations without any need to fit the forces to a surrogate model.

Theories of thermal transport in strongly anharmonic or disordered systems, violation of particle picture, and importance of interband overlaps

Disordered solids were treated by Allen and Feldman (AF) in the 1990s[5,57,58] with the introduction of a new taxonomy for the heat carriers: Propagons, diffusons, and locons. Thermal conductivity was then formulated within the harmonic approximation for diffusons, a majority of the vibrational excitations that do not show any order and have algebraic decay. They are essentially formed from a superposition of local vibrations that have a large real-space overlap allowing to tunnel among themselves due to their energy quasi-degeneracy. There is no clear cut lower-frequency cutoff separating them from propagons, which are wave-like excitations very similar to long wavelength phonons. Simulations have shown that there is a frequency crossover region also called the Ioffe–Regel frequency around which both diffusons and propagons may coexist. It was postulated that it is the frequency at which the propagon is so damped that its mean free path becomes on the order of its wavelength: $\lambda \simeq l_{\mathrm{MFP}}$. It may also be estimated from the structure factor where the peak frequency becomes on the order of the peak broadening $\omega \simeq \gamma(\omega)$. In practice, this is hardly achieved as $\gamma(\omega) \propto \omega^2$. The determination of the cutoff frequency may be a subtle issue that requires further investigation.[59] There is, however, a sharp separation called the mobility edge between the diffusons and locons, which are localized modes occurring near the band edges, with exponential decay. Within the harmonic approximation, locons do not contribute to the thermal conductivity, but if anharmonicity is taken into account, localized energy can hop through coupling with diffusons or propagons from a given site to neighboring sites. Within the AF theory, the contribution of propagons must be separated. It requires the calculation of the Ioffe–Regel cutoff frequency, and, similar to phonons, the speed of sound and a finite MFP or relaxation time for which usually a phenomenological formula of the form $\frac{1}{\tau_{\mathrm{propagon}}} = A\omega^2 T$ can be adopted.

More recently, starting from the Green–Kubo formula and calculating the heat current for a lattice dynamical model (harmonic terms), Isaeva et al.[60] showed that even for strong disorder, a purely harmonic model will have a divergent thermal conductivity. This is because there will be terms such as $cos\omega t$ in the heat current leading to divergent integrals of the type $\int_0^\infty \cos^2\omega t dt$. This result was also previously known by AF and even earlier by Flicker and Leath.[61] This divergence can be resolved if one allows an imaginary part for the mode frequencies reflecting their finite lifetime due to the presence of anharmonicity. In this case, the kinetic BTE formula for the thermal conductivity was extended to disordered systems and labeled quasi-harmonic Green–Kubo (QHGK) formulation.[60] The velocity terms were generalized to matrices. Heat capacity and lifetimes were also generalized to a two-mode version, keeping the overall form of the κ formula the same. They further showed that in the limit of vanishing disorder the standard kinetic formula for κ is recovered.[57,61–63] The QHGK formalism was further extended by Fiorentino and Baroni,[62] based on the Mori–Zwanzig memory formalism and Green–Kubo formula.

As previously mentioned, if the scattering rates, which in the simplest picture are the inverse lifetime or broadening of a phonon state, are large, they can lead to a not so well-defined "independent" phonon state, if, for instance, the difference between two phonon energies ω, ω' becomes smaller than the broadening γ caused by anharmonicity or disorder. The true quantum state would be a superposition of the individual states of energy within γ. In that sense, it is a "coherent" state since the phases of the two modes which were originally unrelated are now the same within the coherence time of $1/\gamma$. This happens in a so-called strong-coupling regime in which perturbative treatments fail. In this case, the standard kinetic approach of BTE also becomes invalid. To remedy this situation, Simoncelli et al. recently adopted the density matrix formalism[59] and later the Wigner distribution function approach[63] to solve the phonon transport equation. The outcome of this treatment is that the velocity now becomes a matrix in the band representation and that total thermal conductivity becomes the sum of the old BTE exact solution plus a correction term, called the coherence contribution, involving the off-diagonal terms in the velocity matrix, phonon frequencies, self-energies, and heat capacities.

$$\kappa^{\alpha\beta} = \frac{1}{N_q \Omega_0}\left[\sum_{q,\lambda} C_{q\lambda} v^{\alpha}_{q\lambda} F^{\beta}_{q\lambda} + \sum_{q,\lambda\neq\lambda'} \int \frac{d^3q}{(2\pi)^3}\left(\frac{C_{q\lambda}}{\omega_{q\lambda}} + \frac{C_{q\lambda'}}{\omega_{q\lambda'}}\right)\frac{\omega_{q\lambda}+\omega_{q\lambda'}}{4} v^{\alpha}_{q,\lambda\lambda'} v^{\beta}_{q,\lambda'\lambda} \mathrm{L}(q,\lambda\lambda')\right], \quad (3)$$

with $\mathrm{L}(q,\lambda\lambda') = \frac{\frac{1}{2}(\Gamma_{q\lambda}+\Gamma_{q\lambda'})}{\left(\omega_{q\lambda}-\omega_{q\lambda'}\right)^2+\frac{1}{4}\left(\Gamma_{q\lambda}+\Gamma_{q\lambda'}\right)^2}$ and $\mathrm{F}_{q\lambda}$ = exact solution to standard (diagonal) BTE.

The first term is the standard solution to BTE (could be within the relaxation time approximation (RTA) or from direct diagonalization/inversion of the collision matrix). It is simple enough to implement within existing transport codes. The coherence term increases with increasing temperature and increasing disorder. This approach becomes also very convenient in inhomogeneous or disordered systems when the very concept of wave vector-resolved phonon becomes questionable. This formalism was applied with success to several anharmonic systems[64] and glasses.[65] The new Wigner formulation has bypassed the need to separate the propagons from diffusons and have produced the thermal conductivity of amorphous silicon within a unified formalism.[66] This formalism produces results very similar to the work of Baroni's group.[67] Differences were shown to be on the order of Γ^2/ω^2.

Hydrodynamic transport regime

Recent advances in first-principles modeling of thermal transport have enabled detailed investigations into phonon scattering processes and relaxation dynamics in various materials.[68,69] In particular, these advances have provided clear evidence—both experimentally and theoretically—for ballistic transport in short samples and hydrodynamic phonon transport at low temperatures and sufficiently small length scales.[70]

A deep understanding of phonon heat transport can be achieved by investigating the collision matrix, first studied systematically by Guyer and Krumhansl.[71,72] They realized that the first four eigenstates of the normal (i.e., momentum conserving) part of the collision matrix have the general drifting form, which can be expanded on eigenstates of the normal collision operator:

$$\left[e^{\beta\hbar(\omega_q - \boldsymbol{q}\cdot\boldsymbol{v}_D)} - 1\right]^{-1} \simeq f_0 + q_x v_{xD} f_{1x} + q_y v_{yD} f_{1y} + q_z v_{zD} f_{1z}\,. \quad (4)$$

Here, $\boldsymbol{q}$ and ω_q are the phonon wavevector and frequency, β is the inverse temperature, and $\boldsymbol{v}_D$ is the drift velocity vector. It can be determined from the constraint of crystal momentum, which is what Callaway used.[2] All modes q have the same drift velocity, implying that any distribution function made as a superposition of these four basis set represents a collective motion of phonons. In reality, the collision matrix is not normal and has a resistive part as well. However, in the limit where resistive terms are small ($\tau_R \gg \tau_N$) (i.e., in clean samples and at low temperatures with few Umklapp processes), to a good approximation the drifting distribution is solution to the BTE, at least until times $t \leq \tau_R$ after which they are damped and relax to the equilibrium BE distribution.

Hydrodynamic or fluid-like flow behavior is then observable when the rates resistive (i.e., nonmomentum-conserving) processes are significantly smaller than those of normal processes denoted by $\Gamma_{q,N} = \frac{1}{\tau_{q,N}}$. Therefore, clean, defect-free samples with minimal resistive scattering clearly exhibit hydrodynamic phonon transport due to the slower decay of collective modes compared to resistive modes.

More recently, Alvarez et al.[73] developed a phenomenological approach called the kinetic collective model (KCM) to treat the hydrodynamic transport of phonons. They separated the mode contribution to the thermal conductivity into a weighted sum of kinetic, where, as in the RTA, each phonon mode contributes some $C_q v_q^2 \tau_q/3$ amount to the thermal conductivity through nonmomentum-conserving processes and collective, which captures hydrodynamic transport. The weight corresponding to each term is proportional to the average resistive and normal rates, respectively, $\kappa = (\kappa_{kin}\Gamma_R + \kappa_{col}\Gamma_N)/(\Gamma_R + \Gamma_N)$. The assumption is that there is a gap between the normal rate of drifting distribution and that of resistive modes, so that collective and kinetic contributions can be well separated. It therefore requires very clean samples. This theory is computationally more tractable than the full solution to BTE, especially for complex materials.

In subsequent work, Alvarez et al. proposed an ansatz[74,75] wherein each phonon mode distribution is the equilibrium distribution plus terms linear in heat flux $\boldsymbol{Q}$ and its time and space derivatives:

$$f_q = f_q^0 + \boldsymbol{A_q}.\boldsymbol{Q} + \boldsymbol{B_q}.\frac{\partial \boldsymbol{Q}}{\partial t} + \boldsymbol{G_q} : \nabla \boldsymbol{Q} \quad (5)$$

and where the mode-dependent coefficient vectors $\boldsymbol{A_q}, \boldsymbol{B_q}\boldsymbol{G_q}$ are determined from conservation equations. This flux derivatives formalism led to a modified Fourier Law, the hyperbolic (Maxwell–Cattaneo) heat equation. The second term guarantees a response linear to the heat flux, and the third allows a wave-like solution (second sound). Coupled with the energy conservation, one obtains a macroscopic heat wave equation, the parameters of which could be expressed in terms of phonon frequencies, group velocities, and RTA relaxation times:

$$C\frac{\partial T}{\partial t} + \nabla.\boldsymbol{Q} = 0;\ \boldsymbol{Q} = -\tau\frac{\partial \boldsymbol{Q}}{\partial t} - \kappa\nabla T + l^2\left[\nabla^2\boldsymbol{Q} + \alpha\nabla(\nabla.\boldsymbol{Q})\right]. \quad (6)$$

Solutions of this modified heat equation with a new length scale l, of relevance for the observation of hydrodynamic effects, by the finite element method (FEM), have been able to explain many experimental observations, such as Poiseuille flow,[75,76] bridging different transport regimes and explaining size effects, including the Knudsen minimum in materials such as Si[77] and second sound in Germanium.[76] Coefficients l, α, τ, κ

are geometry independent and can be calculated from the solution of BTE for the bulk material.

In parallel, Cepellotti and Marzari undertook a more systematic approach using as a representation of the distribution function the full eigenstates of the collision matrix, termed "relaxons."[78–80] This method has clarified and generalized older theories by Callaway[2] and Guyer Krumhansl.[71,81] Callaway associated a relaxation time τ_N to the normal processes that relax to the drifting distribution and another one to the resistive or Umklapp ones τ_R, relaxing to the equilibrium BE distribution, so that the total relaxation time is given by $\frac{1}{\tau} = \frac{1}{\tau_N} + \frac{1}{\tau_R}$. This approach works mostly well in high-thermal-conductivity materials, with some exceptions as explained in the recent work by Ravichandran.[36] Other relaxon modes do also contribute to the thermal transport. At low temperatures, Ravichandran[82] demonstrated that, at low temperatures, only about 3% of relaxon modes are sufficient to capture over 99% of the thermal conductivity in diamond at 100 K, whereas approximately 50% are needed at 300 K.

Simoncelli et al. could derive macroscopic viscous heat equations which, similarly, could be solved by FEM.[83,84]

Boltzmann transport theory solvers implementations

For electronic transport, the transport distribution function is calculated from the band structure (wannierized[85–87] or not). The codes BOLTZTRAP[88,89] and BOLTZWANN[90] perform a constant relaxation time approximation. Electron relaxation mechanisms are implemented in the codes AMSET,[91] ELECTRA,[92] and QUANTUM-ATK.[93]

For phonon transport, many codes are also available. First harmonic and anharmonic force constants are extracted. FOCEX as a part of ALATDYN,[94] HIPHIVE[95] and PHONOPY[54,55] are such codes which use DFT calculations of forces versus displacements in a supercell as input and provide harmonic and anharmonic force constants as output to be processed by other codes (see flowchart in **Figure 3**). Other codes such as SHENG-BTE,[37,53] ALAMODE,[51,52,96] TDEP,[97–99] KALDO,[100] SSCHA,[101–103] THERMACOND, and PHONO3PY[55,104] may do both force constant extraction and thermal conductivity calculation.

Finally, ELPHBOLT[105] and PHOEBE[106] are full implementations of the coupled electron–phonon Boltzmann solver and take as input electron and phonon dispersions, anharmonicities, as well as their coupling constants calculated by codes, such as EPW[24,25,107] and PERTURBO,[26] and calculate the distribution function for both carriers subject to a thermal gradient and voltage. In an impressive paper, Coulter et al.[108] recently developed and solved a hydrodynamic version of the coupled electron–phonon transport problem, and the corresponding code SOLVITE has been interfaced with PHOEBE.

Advances in thermal transport measurements

While the standard way of measuring thermal conductivity of bulk thermoelectric materials remains to be the laser flash method, there has been great advances over the last few decades in the methods to measure local thermal conductivity in micro- and nanoscale regions. One of the most popular approaches has been the pump-probe optical method mostly using thermoreflectance (time-domain themoreflectance, TDTR)[109–111] but some using temperature dependence of Kerr rotation angle (Time-resolved magneto-optical Kerr effect, TR-MOKE)[112] or Raman shift (Flash Raman, FR).[113] They enabled measuring thermal conductivity of thin films and thermal conductance at solid interfaces. Methods using microfabricated devices have also been performed by some researchers although they require more complex processes;[114] a sample is suspended between micro-islands equipped with heaters and thermometers realizing steady-state thermal conductivity measurement of thin films and nanomaterials. The methods are primarily used to measure cross-plane thermal conductivity of thin films, but they can also measure in-plane thermal conductivity when sufficient sensitivity is achieved by offsetting the pump and probe beam[115] or varying the dimension of heat conduction through laser spot size of modulation frequency.[116] The material selectivity of Raman scattering has been used to measure monolayer two-dimensional material thermal conductivity even when supported by the substrate.

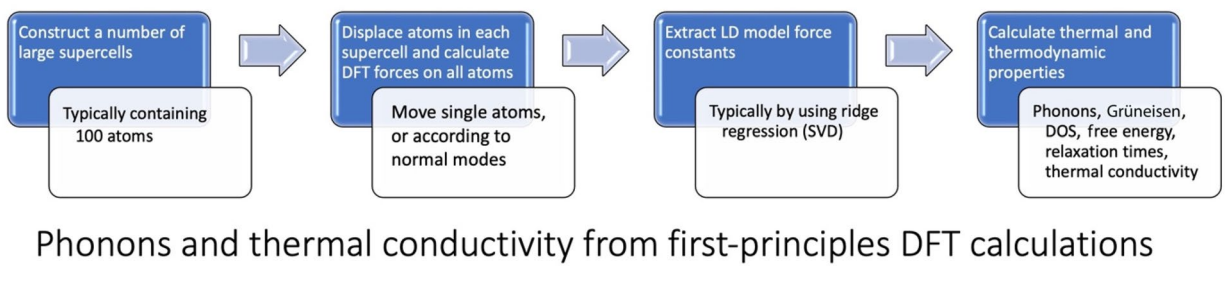

Figure 3. Flowchart of anharmonic force constants and thermal conductivity calculations. DFT density functional theory; LD lattice dynamics; DOS density of states; SVD singular value decomposition.

One merit of the pump-probe method is that it can probe effective thermal conductivity of various sizes by changing the laser spot size, pulse width, or modulation frequency. The size effect measurement has been used to extract the dependence of thermal conductivity on the phonon mean free path.[117,118] Another merit is the facileness to perform mapping of thermal conductivity by traversing the laser spots along the sample surface. This allows obtaining information on uniformity or it can be used for high-throughput screening of combinatorial samples.[119] Furthermore, the mapping measurements of thermal conductivity have been recently used to extract thermal boundary conductance of polycrystal grain boundaries.[120,121] Working on the smoothened cross section of polycrystalline material, when profiling thermal conductivity crossing orthogonally a grain boundary, thermal conductivity drops around the interface with a certain width related to the phonon mean free path. Then, the thermal boundary resistance (inverse thermal conductance) can be extracted by integrating the thermal resistivity (inverse thermal conductivity).

Mode-resolved phonon transport characteristics are measured by inelastic neutron scattering (INS) or inelastic x-ray scattering (IXS), where the line shape and width of the dynamical structural factor give states and the scattering rate of phonons, respectively. Recent development of the instrumentation enabled IXS measurements of thin films by making the incident angle extremely low.[122] In addition, the advanced energy resolution enabled extraction of the electron–phonon scattering rate of doped silicon.[123]

Summary

In summary, this article outlines fundamental concepts, recent theoretical developments, and advanced experimental techniques in thermal transport for thermoelectric materials. Initially, mechanisms of phonon scattering and their dependence on atomic-level details such as chemical bonding and interfaces were discussed. We clearly distinguished between diffusive, hydrodynamic, and ballistic transport regimes and emphasized phonon coherence and scattering processes.

Theoretical models, including Green–Kubo, BTE, and Allen–Feldman theory, along with their modern extensions, were reviewed, highlighting their effectiveness in describing various materials and phenomena such as phonon localization and strong anharmonicity.

Experimental advancements, particularly in nanoscale thermoreflectance (TDTR/FDTR) and Raman spectroscopy, alongside mode-resolved techniques such as inelastic x-ray scattering (IXS), have provided valuable insights into phonon dynamics and thermal transport mechanisms.

For thermoelectric materials, strategies to reduce thermal conductivity by introducing interfaces, defects, and exploiting phonon coherence in superlattices were discussed. Notably, the observation of minima in thermal conductivity versus superlattice period illustrates the balance between coherent and incoherent phonon transport.

Overall, combined theoretical and experimental progress continues to enhance fundamental understanding and guide the development of efficient thermoelectric materials.

Author contributions

Both authors equally contributed to the writing of this review.

Funding

K.E. would like to acknowledge financial support from NSF-CSSI Award No. 2103989. J.S. would like to acknowledge support from CREST Grant No. JPMJCR21O2 from the Japan Science and Technology Agency (JST).

Conflict of interest

The authors declare no conflict of interest.

Open Access

This article is licensed under a Creative Commons Attribution 4.0 International License, which permits use, sharing, adaptation, distribution and reproduction in any medium or format, as long as you give appropriate credit to the original author(s) and the source, provide a link to the Creative Commons licence, and indicate if changes were made. The images or other third party material in this article are included in the article's Creative Commons licence, unless indicated otherwise in a credit line to the material. If material is not included in the article's Creative Commons licence and your intended use is not permitted by statutory regulation or exceeds the permitted use, you will need to obtain permission directly from the copyright holder. To view a copy of this licence, visit http://creativecommons.org/licenses/by/4.0/.

References

1. H. Casimir, *Physica V* **6**, 495 (1938)
2. J. Callaway, *Phys. Rev.* **113**, 1046 (1959)
3. M. Asheghi, Y.K. Leung, S.S. Wong, K.E. Goodson, *Appl. Phys. Lett.* **71**, 1798 (1997)
4. M. Asheghi, K. Kurabayashi, R. Kasnavi, K.E. Goodson, *J. Appl. Phys.* **91**, 5079 (2002)
5. P.B. Allen, J.L. Feldman, *Phys. Rev. B* **48**, 12581 (1993)
6. E.H. Sondheimer, *Adv. Phys.* **50**, 499 (1952)
7. M. Maldovan, *J. Appl. Phys.* **111**, 024311 (2012)
8. M. Maldovan, *Appl. Phys. Lett.* **101**, 113110 (2012)
9. N. Mingo, *Phys. Rev. B Condens. Matter Mater. Phys.* **68**, 113308 (2003)
10. P. Martin, Z. Aksamija, E. Pop, U. Ravaioli, *Phys. Rev. Lett.* **102**, 125503 (2009)
11. S. Tamura, *Phys. Rev. B* **27**, 858 (1983)
12. I. Savić, N. Mingo, D.A. Stewart, *Phys. Rev. Lett.* **101**, 165502 (2008)
13. M. Arrigoni, J. Carrete, N. Mingo, G.K.H. Madsen, *Phys. Rev. B* **98**, 115205 (2018)
14. A. Kundu, N. Mingo, D.A. Broido, D.A. Stewart, *Phys. Rev. B Condens. Matter Mater. Phys.* **84**, 125426 (2011)
15. N. Mingo, K. Esfarjani, D.A. Broido, D.A. Stewart, *Phys. Rev. B Condens. Matter Mater. Phys.* **81**, 045408 (2010)
16. N. Mingo, D. Hauser, N.P. Kobayashi, M. Plissonnier, A. Shakouri, *Nano Lett.* **9**, 711 (2009)
17. A. Granato, K. Lücke, *J. Appl. Phys.* **27**, 583 (1956)
18. M. Li, *J. Phys. Condens. Matter* **31**, 083001 (2019)
19. M. Li, Y. Tsurimaki, Q. Meng, N. Andrejevic, Y. Zhu, G.D. Mahan, G. Chen, *New J. Phys.* **20**, 023010 (2018)
20. J. Mendoza, K. Esfarjani, G. Chen, *J. Appl. Phys.* **117**, 174301 (2015)
21. J. Garg, N. Bonini, N. Marzari, *Nano Lett.* **11**, 5135 (2011)
22. K. Esfarjani, J. Garg, G. Chen, "Modeling Heat Conduction from First Principles," in *Annual Review of Heat Transfer*, vol. 17, ed. by Z.M. Zhang, V. Prasad, Y. Jaluria (Begell House, Danbury, 2014), pp. 9–47
23. R.J. Elliott, J.A. Krumhansl, P.L. Leath, *Rev. Mod. Phys.* **46**, 465 (1974)

24. F. Giustino, *Rev. Mod. Phys.* **89**, 015003 (2017)
25. S. Poncé, E.R. Margine, C. Verdi, F. Giustino, *Comput. Phys. Commun.* **209**, 116 (2016)
26. J.J. Zhou, J. Park, I. Te Lu, I. Maliyov, X. Tong, M. Bernardi, *Comput. Phys. Commun.* **264**, 107970 (2021)
27. P. Sun, N. Oeschler, S. Johnsen, B.B. Iversen, F. Steglich, *J. Phys. Conf. Ser.* **150**, 012049 (2009)
28. M.S. Diakhate, R.P. Hermann, A. Möchel, I. Sergueev, M. Søndergaard, M. Christensen, M.J. Verstraete, *Phys. Rev. B Condens. Matter Mater. Phys.* **84**, 125210 (2011)
29. M. Pokharel, H. Zhao, K. Lukas, Z. Ren, C. Opeil, B. Mihaila, *MRS Commun.* **3**, 31 (2013)
30. H. Matsuura, H. Maebashi, M. Ogata, H. Fukuyama, *J. Phys. Soc. Jpn.* **88**, 074601 (2019)
31. J. Zhou, B. Liao, B. Qiu, S. Huberman, K. Esfarjani, M.S. Dresselhaus, G. Chen, *Proc. Natl. Acad. Sci. U.S.A.* **112**(48) (2015), pp. 14777–14782
32. G.D. Mahan, L. Lindsay, D.A. Broido, *J. Appl. Phys.* **116**, 245102 (2014)
33. C. Li, N.H. Protik, N.K. Ravichandran, D. Broido, *Phys. Rev. B* **107**, L081202 (2023)
34. C. Herring, *Phys. Rev.* **96**, 1163 (1954)
35. F. Tian, B. Song, X. Chen, N.K. Ravichandran, Y. Lv, K. Chen, S. Sullivan, J. Kim, Y. Zhou, T.-H. Liu, M. Goni, Z. Ding, J. Sun, G.A.G. Udalamatta Gamage, H. Sun, H. Ziyaee, S. Huyan, L. Deng, J. Zhou, A.J. Schmidt, S. Chen, C.-W. Chu, P.Y. Huang, D. Broido, L. Shi, G. Chen, Z. Ren, *Science* **361**, 582 (2018)
36. N. Malviya, N.K. Ravichandran, *Phys. Rev. B* **108**, 155201 (2023)
37. Z. Han, X. Yang, W. Li, T. Feng, X. Ruan, *Comput. Phys. Commun.* **270**, 108179 (2022)
38. P. Hyldgaard, G. Mahan, *Phys. Rev. B Condens. Matter Mater. Phys.* **56**, 10754 (1997)
39. M.V. Simkin, G.D. Mahan, *Phys. Rev. Lett.* **84**, 927 (2000)
40. J. Ravichandran, A.K. Yadav, R. Cheaito, P.B. Rossen, A. Soukiassian, S.J. Suresha, J.C. Duda, B.M. Foley, C.H. Lee, Y. Zhu, A.W. Lichtenberger, J.E. Moore, D.A. Muller, D.G. Schlom, P.E. Hopkins, A. Majumdar, R. Ramesh, M.A. Zurbuchen, *Nat. Mater.* **13**, 168 (2014)
41. S.T. Huxtable, A.R. Abramson, C.L. Tien, A. Majumdar, C. Labounty, X. Fan, G. Zeng, J.E. Bowers, A. Shakouri, E.T. Croke, *Appl. Phys. Lett.* **80**, 1737 (2002)
42. S.M. Lee, D.G. Cahill, R. Venkatasubramanian, *Appl. Phys. Lett.* **70**, 2957 (1997)
43. Y.K. Koh, Y. Cao, D.G. Cahill, D. Jena, *Adv. Funct. Mater.* **19**, 610 (2009)
44. B. Saha, Y.R. Koh, J. Comparan, S. Sadasivam, J.L. Schroeder, M. Garbrecht, A. Mohammed, J. Birch, T. Fisher, A. Shakouri, T.D. Sands, *Phys. Rev. B* **93**, 045311 (2016)
45. M.N. Luckyanova, J. Garg, K. Esfarjani, A. Jandl, M.T. Bulsara, A.J. Schmidt, A.J. Minnich, S. Chen, M.S. Dresselhaus, Z. Ren, E.A. Fitzgerald, G. Chen, *Science* **338**, 936 (2012)
46. M. Khazaei, A. Ranjbar, K. Esfarjani, D. Bogdanovski, R. Dronskowski, S. Yunoki, *Phys. Chem. Chem. Phys.* **20**, 8579 (2018)
47. R. Dronskowski, P.E. Blöchl, *J. Phys. Chem.* **97**, 8617 (1993)
48. J. Yuan, Y. Chen, B. Liao, *J. Am. Chem. Soc.* **145**, 18506 (2023)
49. S. Nayeb Sadeghi, K. Esfarjani, *J. Mater. Chem. A Mater.* **12**, 25067 (2024)
50. L. Elalfy, D. Music, M. Hu, *Phys. Rev. B* **103**, 75203 (2021)
51. T. Tadano, Y. Gohda, S. Tsuneyuki, *J. Phys. Condens. Matter* **26**, 225402 (2014)
52. T. Tadano, S. Tsuneyuki, *J. Phys. Soc. Jpn.* **87**, 041015 (2018)
53. W. Li, J. Carrete, N.A. Katcho, N. Mingo, *Comput. Phys. Commun.* **185**, 1747 (2014)
54. A. Togo, I. Tanaka, *Scr. Mater.* **108**, 1 (2015)
55. A. Togo, *J. Phys. Soc. Jpn.* **92**, 012001 (2023)
56. A. Marcolongo, P. Umari, S. Baroni, *Nat. Phys.* **12**, 80 (2016). https://doi.org/10.1038/nphys3509
57. J.L. Feldman, M.D. Kluge, P.B. Allen, F. Wooten, *Phys. Rev. B* **48**, 12589 (1993)
58. P.B. Allen, J.L. Feldman, *Phys. Rev. Lett.* **62**, 645 (1989)
59. M. Simoncelli, N. Marzari, F. Mauri, *Nat. Phys.* **15**, 809 (2019)
60. L. Isaeva, G. Barbalinardo, D. Donadio, S. Baroni, *Nat. Commun.* **10**, 3853 (2019)
61. J.K. Flicker, P.L. Leath, *Phys. Rev. B* **7**, 2296 (1973)
62. A. Fiorentino, S. Baroni, *Phys. Rev. B* **107**, 054311 (2023)
63. M. Simoncelli, N. Marzari, F. Mauri, *Phys. Rev. X* **12**, 041011 (2022). https://doi.org/10.1103/PhysRevX.12.041011
64. M. Simoncelli, N. Marzari, F. Mauri, *Phys. Rev. X* **12**, 041011 (2022)
65. M. Simoncelli, F. Mauri, N. Marzari, *NPJ Comput. Mater.* **9**, 106 (2023). https://doi.org/10.1038/s41524-023-01033-4
66. J. Yang, X. Zhu, A.J.H. Mcgaughey, Y. Sin Ang, W.-L. Ong, *Phys. Rev. B* **111**, 94206 (2025)
67. S. Baroni, A. Fiorentino, *Phys. Rev. B* **107**, 054311 (2023)
68. X. Li, S. Lee, *Phys. Rev. B* **99**, 075202 (2019)
69. X. Li, H. Lee, E. Ou, S. Lee, L. Shi, *J. Appl. Phys.* **131**, 75104 (2022)
70. S.Y. Lee, X. Li, "Hydrodynamic Phonon Transport: Past, Present, and Prospects," in *Nanoscale Energy Transport: Emerging Phenomena, Methods and Applications* (IOP Publishing, Philadelphia, 2020), pp. 1-1–1-26. https://doi.org/10.1088/978-0-7503-1738-2ch1
71. R.A. Guyer, J.A. Krumhansl, *Phys. Rev.* **148**, 766 (1966)
72. R.A. Guyer, J.A. Krumhansl, *Phys. Rev.* **148**, 778 (1966)
73. C. De Tomas, A. Cantarero, A.F. Lopeandia, F.X. Alvarez, *J. Appl. Phys.* **115**, 164314 (2014)
74. L. Sendra, A. Beardo, P. Torres, J. Bafaluy, F.X. Alvarez, J. Camacho, *Phys. Rev. B* **103**, L140301 (2021)
75. L. Sendra, A. Beardo, J. Bafaluy, P. Torres, F.X. Alvarez, J. Camacho, *Phys. Rev. B* **106**, 155301 (2022)
76. A. Beardo, M. López-Suárez, L.A. Pérez, L. Sendra, M.I. Alonso, C. Melis, J. Bafaluy, J. Camacho, L. Colombo, R. Rurali, F.X. Alvarez, J.S. Reparaz, *Sci. Adv.* **7**, eabg4677 (2021)
77. A. Beardo, J.L. Knobloch, L. Sendra, J. Bafaluy, T.D. Frazer, W. Chao, J.N. Hernandez-Charpak, H.C. Kapteyn, B. Abad, M.M. Murnane, F.X. Alvarez, J. Camacho, *ACS Nano*, **15**, 13019 (2021)
78. A. Cepellotti, N. Marzari, *Phys. Rev. X* **6**, 041013 (2016). https://doi.org/10.1103/PhysRevX.6.041013
79. A. Cepellotti, N. Marzari, *Phys. Rev. Mater.* **1**, 045406 (2017). https://doi.org/10.1103/PhysRevMaterials.1.045406
80. A. Cepellotti, N. Marzari, *Handbook of Materials Modeling* (Springer, Cham, 2020). https://doi.org/10.1007/978-3-319-44680-6_11
81. R.A. Guyer, J.A. Krumhansl, *Phys. Rev.* **148**, 778 (1966)
82. N. Malviya, N.K. Ravichandran, Efficient calculation of phonon dynamics through a low–rank solution of the Boltzmann equation (2025), Preprint, https://doi.org/10.48550/arXiv.2502.00337
83. M. Simoncelli, N. Marzari, A. Cepellotti, *Phys. Rev. X* **10**, 011019 (2020)
84. J. Dragašević, M. Simoncelli, Viscous heat backflow and temperature resonances in extreme thermal conductors (2023), Preprint, https://doi.org/10.48550/arXiv.2303.12777
85. G. Pizzi, V. Vitale, R. Arita, S. Blügel, F. Freimuth, G. Géranton, M. Gibertini, D. Gresch, C. Johnson, T. Koretsune, J. Ibañez-Azpiroz, H. Lee, J.-M. Lihm, D. Marchand, A. Marrazzo, Y. Mokrousov, J.I. Mustafa, Y. Nohara, Y. Nomura, L. Paulatto, S. Poncé, T. Ponweiser, J. Qiao, F. Thöle, S.S. Tsirkin, M. Wierzbowska, N. Marzari, D. Vanderbilt, I. Souza, A.A. Mostofi, J.R. Yates, *J. Phys. Condens. Matter* **32**, 165902 (2019)
86. A.A. Mostofi, J.R. Yates, Y.S. Lee, I. Souza, D. Vanderbilt, N. Marzari, *Comput. Phys. Commun.* **178**, 685 (2008)
87. A.A. Mostofi, J.R. Yates, G. Pizzi, Y.S. Lee, I. Souza, D. Vanderbilt, N. Marzari, *Comput. Phys. Commun.* **185**, 2309 (2014)
88. G.K.H. Madsen, D.J. Singh, *Comput. Phys. Commun.* **175**, 67 (2006)
89. G.K.H. Madsen, J. Carrete, M.J. Verstraete, *Comput. Phys. Commun.* **231**, 140 (2018)
90. G. Pizzi, D. Volja, B. Kozinsky, M. Fornari, N. Marzari, *Comput. Phys. Commun.* **185**, 422 (2014)
91. A.M. Ganose, J. Park, A. Faghaninia, R. Woods-Robinson, K.A. Persson, A. Jain, *Nat. Commun.* **12**, 2222 (2021)
92. P. Graziosi, Z. Li, N. Neophytou, *Comput. Phys. Commun.* **287**, 108670 (2023)
93. S. Smidstrup, T. Markussen, P. Vancraeyveld, J. Wellendorff, J. Schneider, T. Gunst, B. Verstichel, D. Stradi, P.A. Khomyakov, U.G. Vej-Hansen, M.E. Lee, S.T. Chill, F. Rasmussen, G. Penazzi, F. Corsetti, A. Ojanperä, K. Jensen, M.L.N. Palsgaard, U. Martinez, A. Blom, M. Brandbyge, K. Stokbro, *J. Phys. Condens. Matter* **32**, 015901 (2019)
94. K. Esfarjani, H. Stokes, S. Nayeb Sadeghi, Y. Liang, B. Timalsina, H. Meng, J. Shiomi, B. Liao, R. Sun, *Comput. Phys. Commun.* **312**, 109575 (2025)
95. F. Eriksson, E. Fransson, P. Erhart, *Adv. Theory Simul.* **2**, 1800184 (2019)
96. T. Tadano, S. Tsuneyuki, *Phys. Rev. B* **92**, 054301 (2015)
97. O. Hellman, I.A. Abrikosov, S.I. Simak, *Phys. Rev. B Condens. Matter Mater. Phys.* **84**, 180301 (2011)
98. O. Hellman, I.A. Abrikosov, *Phys. Rev. B* **88**, 144301 (2013)
99. O. Hellman, P. Steneteg, I.A. Abrikosov, S.I. Simak, *Phys. Rev. B Condens. Matter Mater. Phys.* **87**, 104111 (2013)
100. G. Barbalinardo, Z. Chen, N.W. Lundgren, D. Donadio, *J. Appl. Phys.* **128**, 135104 (2020). https://doi.org/10.1063/5.0020443
101. L. Monacelli, R. Bianco, M. Cherubini, M. Calandra, I. Errea, F. Mauri, *J. Phys. Condens. Matter* **33**(36), 363001 (2021). https://doi.org/10.1088/1361-648X/ac066b
102. L. Paulatto, I. Errea, M. Calandra, F. Mauri, *Phys. Rev. B* **91**, 54304 (2015)
103. I. Errea, M. Calandra, F. Mauri, *Phys. Rev. B* **89**, 64302 (2014)
104. A. Togo, L. Chaput, T. Tadano, I. Tanaka, *J. Phys. Condens. Matter* **35**, 353001 (2023)
105. N.H. Protik, C. Li, M. Pruneda, D. Broido, P. Ordejón, *NPJ Comput. Mater.* **8**, 28 (2022)
106. A. Cepellotti, J. Coulter, A. Johansson, N.S. Fedorova, B. Kozinsky, *J. Phys. Mater.* **5**, 035003 (2022)
107. P. Giannozzi, O. Andreussi, T. Brumme, O. Bunau, M. Buongiorno Nardelli, M. Calandra, R. Car, C. Cavazzoni, D. Ceresoli, M. Cococcioni, N. Colonna, I. Carnimeo, A. Dal Corso, S. De Gironcoli, P. Delugas, R.A. Distasio, A. Ferretti, A. Floris, G. Fratesi, G. Fugallo, R. Gebauer, U. Gerstmann, F. Giustino, T. Gorni, J. Jia, M. Kawamura, H.Y. Ko, A. Kokalj, E. Küçükbenli, M. Lazzeri, M. Marsili, N. Marzari, F. Mauri, N.L. Nguyen, H.V. Nguyen, A. Otero-De-La-Roza, L. Paulatto, S. Poncé, D. Rocca, R. Sabatini, B. Santra, M. Schlipf, A.P. Seitsonen, A. Smogunov, I. Timrov, T. Thonhauser, P. Umari, N. Vast, X. Wu, S. Baroni, *J. Phys. Condens. Matter* **29**(46), 465901 (2017). https://doi.org/10.1088/1361-648X/aa8f79
108. J. Coulter, B. Rajkov, M. Simoncelli, Coupled electron-phonon hydrodynamics and viscous thermoelectric equations (2025), Preprint, https://doi.org/10.48550/arXiv.2503.07560
109. W.S. Capinski, H.J. Maris, *Rev. Sci. Instrum.* **67**, 2720 (1996)

110. N. Taketoshi, T. Baba, E. Schaub, A. Ono, *Rev. Sci. Instrum.* **74**, 5226 (2003)
111. D.G. Cahill, *Rev. Sci. Instrum.* **75**, 5119 (2004)
112. J. Liu, G.M. Choi, D.G. Cahill, *J. Appl. Phys.* **116**, 233107 (2014)
113. Q.Y. Li, X. Zhang, Y.D. Hu, *Thermochim. Acta* **592**, 67 (2014)
114. P. Kim, L. Shi, A. Majumdar, P.L. McEuen, *Phys. Rev. Lett.* **87**, 215502 (2001)
115. J.P. Feser, D.G. Cahill, *Rev. Sci. Instrum.* **83**, 104901 (2012). https://doi.org/10.1063/1.4757863
116. A.J. Schmidt, R. Cheaito, M. Chiesa, *Rev. Sci. Instrum.* **80**, 40 (2009)
117. A.J. Minnich, J.A. Johnson, A.J. Schmidt, K. Esfarjani, M.S. Dresselhaus, K.A. Nelson, G. Chen, *Phys. Rev. Lett.* **107**, 095901 (2011)
118. K.T. Regner, D.P. Sellan, Z. Su, C.H. Amon, A.J.H. McGaughey, J.A. Malen, *Nat. Commun.* **4**, 1640 (2013)
119. S. Huxtable, D.G. Cahill, V. Fauconnier, J.O. White, J.C. Zhao, *Nat. Mater.* **3**, 298 (2004)
120. E. Isotta, S. Jiang, G. Moller, A. Zevalkink, G.J. Snyder, O. Balogun, *Adv. Mater.* **35**, 2302777 (2023)
121. E. Isotta, S. Jiang, R. Bueno-Villoro, R. Nagahiro, K. Maeda, D.A. Mattlat, A.R. Odufisan, A. Zevalkink, J. Shiomi, S. Zhang, C. Scheu, G.J. Snyder, O. Balogun, *Adv. Funct. Mater.* **34**, 2405413 (2024)
122. H. Uchiyama, Y. Oshima, R. Patterson, S. Iwamoto, J. Shiomi, K. Shimamura, *Phys. Rev. Lett.* **120**, 235901 (2018)
123. H. Uchiyama, T.H. Liu, T. Ono, J. Fujise, B. Liao, S. Ju, G. Chen, J. Shiomi, *Phys. Rev. Mater.* **7**, 104601 (2023) □

Publisher's note Springer Nature remains neutral with regard to jurisdictional claims in published maps and institutional affiliations.

Keivan Esfarjani is an associate professor in the Department of Materials Science and Engineering at the University of Virginia and is a theoretical and computational materials scientist. He specializes in phonon transport, thermoelectric materials, and density functional theory. He pioneered methods to compute phonon lifetimes and thermal conductivity from first principles. Educated in France and the United States, he has held positions at the Massachusetts Institute of Technology and the University of California, Santa Cruz, contributing significantly to nanoscale heat and charge-transport modeling. Esfarjani can be reached by email at kl@virginia.edu.

Junichiro Shiomi is a professor in the Institute of Engineering Innovation and the Department of Mechanical Engineering at The University of Tokyo, Japan. He leads the Thermal Energy Engineering Laboratory, focusing on nanoscale heat transfer, thermoelectric energy conversion, and materials informatics. He earned his PhD degree from the Swedish Royal Institute of Technology (KTH) in 2004 and has held roles, including assistant dean and visiting researcher at the Massachusetts Institute of Technology. His work advances sustainable energy technologies through multiscale thermal engineering. Shiomi can be reached by email at shiomi@photon.t.u-tokyo.ac.jp.